RESEARCH ARTICLE

Influence of binder content in silver-based gas diffusion electrodes on pore system and electrochemical performance

David Franzen[1] · Barbara Ellendorff[1] · Melanie C. Paulisch[2] · André Hilger[2] · Markus Osenberg[2] · Ingo Manke[2] · Thomas Turek[1]

Abstract

The influences of the polytetrafluoroethylene (PTFE) content in silver-based gas diffusion electrodes on the resulting physical properties and the electrochemical performance during oxygen reduction in concentrated sodium hydroxide electrolyte were investigated through half-cell measurements. A systematic variation of the pore system was achieved by application of different silver/PTFE ratios during the production of the gas diffusion electrodes (GDE). In all electrodes, a silver skeleton structure with relatively constant properties was formed, while the PTFE fills up part of the open pore space. The resulting structures were characterized with a variety of methods for the physical properties supported by focused ion beam milling and scanning electron microscope (FIB/SEM) tomography. It could be shown that variations in the obtained pore system strongly influence the electrochemical performance of the electrodes. Determination of the Tafel slopes revealed that this is not due to changes in the electrocatalytic activity but rather caused by variations in the electrolyte uptake. While too small amounts of PTFE (1 wt%) lead to decreased performance through electrolyte flooding, higher PTFE contents above about 5 wt% also deteriorate the electrode performance because the extent of the three-phase boundary diminishes. The decisive role of the electrolyte intrusion was confirmed by measurements at higher electrolyte pressure. While the best electrochemical performance was achieved with an electrode containing 98 wt% silver, a slightly higher PTFE content is advisable to prevent breakthrough of the electrolyte.

Graphical abstract
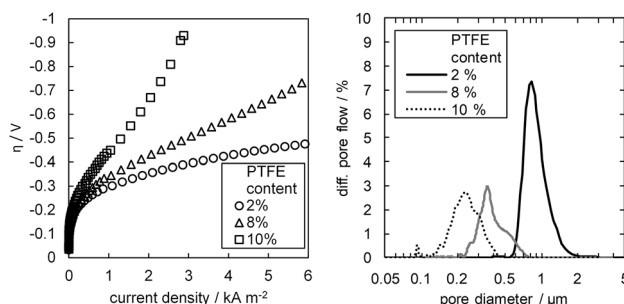
Keywords Oxygen reduction reaction · Gas diffusion electrode · Chlor-alkali electrolysis · Oxygen depolarized cathode · Silver

1 Introduction

The global chlorine production is mainly based on the chlor-alkali electrolysis, which is one of the most energy-intensive processes in the chemical industry [1]. During the classical variant of the electrolysis process, chlorine

✉ David Franzen
  franzen@icvt.tu-clausthal.de

Extended author information available on the last page of the article

gas is formed at the anode, while hydroxide ions are produced together with hydrogen gas at the cathode. A significant reduction of the electrical energy demand of this process was obtained by introducing a gas diffusion electrode (GDE) to the process resulting in oxygen reduction at the cathode rather than hydrogen evolution. The achievable cell voltage decreases of approximately 1 V lead to electrical energy savings of up to 30% of this so-called oxygen depolarized cathode (ODC) technology [2]. The development of processes and suitable catalyst materials for the required GDE have already been discussed in previous work [3]. Despite intensive research over several decades, the stability of carbon-based materials has proven to be insufficient under the harsh process conditions during technical electrolysis (80–90 °C, 30–32 wt% NaOH). On the other hand, silver has a similarly good activity for the oxygen reduction reaction (ORR) under these conditions [4]. Hence, commercial GDE for ODC electrolysis is carbon- and platinum-free and is based on silver as electrocatalyst.

In previous work, variations of silver raw materials and compositions of silver-based GDE lead to optimized electrodes regarding energy consumption and long-term stability [5]. However, proper structure–property relationships explaining why certain electrodes perform better than others are still lacking. Furthermore, models describing the processes within the GDE [6] and ODC chlor-alkali electrolysis cells [7] were developed. These simulations revealed that especially at high current densities, an insufficient supply of oxygen at the surface of the electrocatalyst occurs. That would mean that mass transport rather than the electrochemical activity is the limiting factor in these electrodes. This assumption is supported by findings obtained with electrodes containing very low amounts of the silver catalyst in dendritic form. These materials also revealed excellent performance, however at the expense of lower long-term stability [8]. It can be expected that a proper characterization of the pore system and the processes in the pores offer further major potential for improvement of silver-based GDE.

An efficient tool in the visualization of internal pore structures is the focused ion beam (FIB) tomography combined with a scanning electron microscope (SEM) [9]. On the basis of this image data, reconstructions of the pore system as 3D models coupled with numerical simulations of the transport processes are possible [10]. The disadvantages are that the provided image sections are rather small and offer only a limited overview. For the GDE examined in this work, a stochastic model based on FIB tomography was developed that represents the structure on a larger scale [11]. The structure serves as a basis for further numerical simulations considering, for example, transport phenomena inside the electrode. However, such large-scale simulations still pose challenges to modern computing systems.

Therefore, in this contribution the physical and electrochemical properties of silver-based GDE are analyzed using established characterization methods [12] supported by FIB tomography and the generated 3D reconstructions [13]. For a series of electrodes with different composition, the resulting electrochemical performance is determined via half-cell measurements.

2 Experimental

2.1 Electrode preparation

For each electrode, a suspension containing 30 g silver particles (SF9ED, Ferro GmbH) and a PTFE dispersion (TF 5060GZ, 3 M™ Dyneon™) in the desired ratio was prepared. 50 g of a methyl cellulose solution containing 1 wt% hydroxyethylmethyl cellulose (WALOCEL™ MKX 70000 PP 01) and demineralized water was added as pore building agent and thickener. Depending on the GDE composition, a further amount of demineralized water was required to maintain a proper viscosity. The suspension was applied on a nickel mesh as conductive supporting material (106 μm × 118 μm mesh size, 63 μm thickness, Haver & Boecker OHG) using a spraying piston (Evolution, 0.6 mm pin hole, Harder & Steenbeck). For each electrode, 80 coatings were applied on a heating table allowing simultaneous drying leading to the formation of a homogeneous surface [14]. In the subsequent processing steps, the electrode was hot pressed (LaboPress P200S, Vogt, 15 MPa, 130 °C, 5 min) and heat-treated in an air oven (330 °C, 15 min) to burn out the methylcellulose and to improve the mechanical stability through PTFE sintering. Afterwards, the electrode thickness and catalyst load were determined. The mean thickness was obtained from measurements at six points with a thickness dial gauge (FD 50, Käfer GmbH), while the catalyst load was determined by weighing. For industrial applications, silver contents of 92–98 wt% facing the electrolyte side and 95–99.9 wt% facing the gas side, respectively, with catalyst loadings of 140–250 mg cm^{-2} are desired [15]. To investigate a uniform porous layer, only single-layer GDE with silver contents of 90–99 wt% was prepared. A list of the properties for all electrodes produced is provided in Table 1. In the following, the electrodes will be referred to by values for the silver content rounded to full weight percentage points.

2.2 Physical characterization

The true density of the produced electrodes was obtained with a helium pycnometer (Pycnomatic ATC, Quantachrome), which measures the volume of the displaced helium. As the helium penetrates all open pores, the true

Table 1 Overview about electrode properties

Silver content wt%	Silver load mg cm^{-2}	PTFE load mg cm^{-2}	Thickness μm
99.0	155.7	1.7	356
97.9	150.5	3.2	335
97.0	131.4	4.1	297
96.0	129.1	5.4	293
94.9	125.6	6.8	292
94.0	131.6	8.4	302
93.0	139.9	10.5	321
91.8	138.3	12.3	319
90.8	158.9	16.1	375
89.9	136.9	15.4	330

density is independent of the porosity. On the other hand, the expected density was calculated based on the electrode weight and the true densities of silver (10.49 g cm^{-3}), PTFE (2.2 g cm^{-3}), and nickel (8.91 g cm^{-3}), and should also be independent of the porosity. Flow-through pores and bubble point pressure were determined using capillary flow porometry (Porometer 3G, Quantachrome). A wetting fluid (Porofil, Quantachrome) was applied to the probe which was adjusted in the device. Afterwards, the fluid was driven out of the pores with a pressure gradient. The resulting nitrogen flow was detected on top of the probe. The bubble point pressure was determined at a nitrogen flow rate of 0.1 L min^{-1}. The flow-through pore distribution was finally determined by comparing the nitrogen flow through the wet and dry probe. Specific surface areas of the electrodes were determined using the BET method (3 Flex, Micromeritics Instrument Corp.) with krypton as a sample gas. This minimized the device error in view of the small overall inner surface area. Mercury porosimetry (Pascal 140 + 440, Thermo Fisher Scientific) measurements were tested as an additional method, but due to amalgam formation, reproducible results could not be obtained. Visualization of the microstructure inside the electrodes was investigated by means of FIB milling combined with SEM. Segments with a size of 2 mm × 4 mm were extracted mechanically from the center of the GDE and fixed on SEM sample holders with carbon pads. For ion cutting, a Zeiss Crossbeam 340 Gallium-FIB/SEM device was used. The coarse cut was done using an acceleration voltage of 30 keV and an ion current of 50 nA. For the final polishing setup, 30 keV and 700 pA were employed. The silver fraction in the GDE microstructure was calculated with the imaging software Fiji [16].

2.3 Electrochemical characterization

Electrochemical properties were determined in half-cell measurements (FlexCell HZ-PP01, Gaskatel GmbH) at

80 °C using 30 wt% NaOH as electrolyte prepared from caustic flakes (≥ 99 wt%, Carl Roth) and demineralized water. All reported current densities are related to the geometric cell area of 3.14 cm^2. Experiments were performed with a Zennium Pro Potentiostat (Zahner GmbH). The electrodes were characterized following the same routine, including a start-up procedure and cell resistance determination with pseudo-galvanostatic impedance measurements. Finally, an iR compensated linear sweep voltammetry (LSV) measurement starting at open cell potential (OCP) to 200 mV versus reversible hydrogen electrode (RHE) with a scan rate of 0.5 mV s^{-1} was performed.

The half-cell contained a gas and an electrolyte chamber separated by the GDE. Measurements were performed using a three-electrode configuration with the GDE as working electrode. As the counter electrode, a platinum wire was placed inside the electrolyte chamber with a volume of approximately 30 mL. The potentials were measured in front of the working electrode using a Luggin capillary with a RHE (Hydroflex, Gaskatel GmbH). On the gas side pure oxygen was supplied with a flow rate of 50 mL$_N$ min^{-1} and a small backpressure using a 1 mm water column.

Additional experiments applying an increased electrolyte pressure were performed in a special plant with an electrolyte cycle and separate pressure control for the electrolyte and gas supply. The half-cell design (Fig. 1) is similar to the FlexCell, providing the same electrode configuration. Pressure and temperature on gas and electrolyte side were monitored with sensors. During these experiments, gas and electrolyte pressure were set to 1000 mbar first. Subsequently, the electrolyte pressure was increased stepwise. All other process parameters were kept at the same conditions as during the experiments in the FlexCell.

To determine proper equilibrium potentials of the oxygen reduction reaction (ORR) versus RHE, standard potentials for both reactions were calculated using the Nernst equation. The temperature dependence of the standard potentials was taken into account according to Bratsch [17], while the activities of water [18] and OH$^-$ ions [19] were based on the work of Balej. Additionally partial pressures of hydrogen, at the RHE, and oxygen, at the GDE, were corrected by the water vapor pressure above the NaOH solution at the given temperature [18]. Finally the solubility of oxygen was determined with the model of Tromans [20]. Overall, the standard potential of the ORR vs. RHE could be determined as 1.13 V at the given process conditions.

Evaluation of the LSV measurements was done by determining Tafel slopes and exchange current densities from the polarization curve. As will be shown later, two linear regions on the logarithmic current density scale were observed. This behavior is typical for the ORR in alkaline electrolyte [21] and was observed by Pinnow et al. [6] during their measurements with Ag/PTFE electrodes. While the

Fig. 1 Half-cell for the measurements at elevated electrolyte pressure, electrolyte outlet is located behind the counter electrode
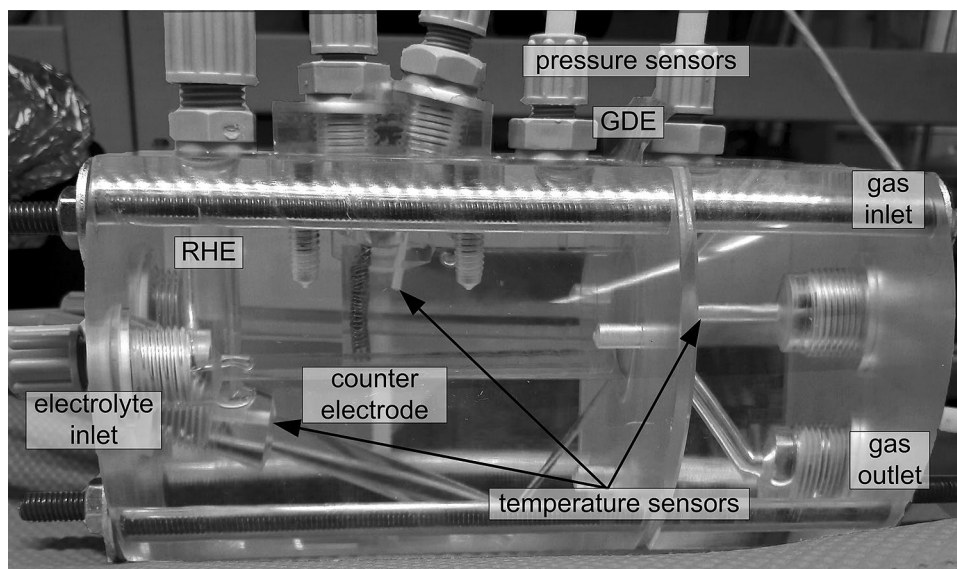
first Tafel slope was obtained for overpotentials between 80 and 120 mV, the second slope refers to overpotentials in the range between 200 and 250 mV. For all measurements, the range was defined individually to maximize the linear correlation factor.

3 Results and discussion

3.1 Influence of PTFE content on pore system

In Fig. 2, the results of the porometry and bubble point measurements are shown for all prepared electrodes. It can be seen that the electrode with the highest silver content (99 wt%) has the largest median pore size of about 1 μm and a relatively sharp pore size distribution. Increasing the PTFE content decreases the pore size and broadens the pore size distribution. For the lowest applied silver content of

90 wt%, the median pore size is decreased to approx. 0.2 μm. The right-hand diagram in Fig. 2 shows that rising PTFE content and thus smaller pores lead to an increase of the bubble point pressure. While the bubble point pressure of the electrode with 99 wt% silver is only 0.5 bar, this value rises strongly reaching 2.5 bar for 90 wt% silver. However, these measurements were performed with a wetting fluid at room temperature and bubble points could differ when using the electrolyte at process conditions. Furthermore, electrowetting effects are not considered [22]. Nevertheless, the bubble point pressure is a good indicator for the wettability at process conditions. A low value will probably lead to a complete flooding of the electrode and thus higher transport resistance through the electrolyte. High values could correspond to severe blocking of the electrolyte paths inside providing only minimal electrolyte penetration. In both cases, the accessible reactive surface of the GDE would be strongly reduced.

Fig. 2 Results of capillary flow porometry and bubble point for electrodes with different silver contents
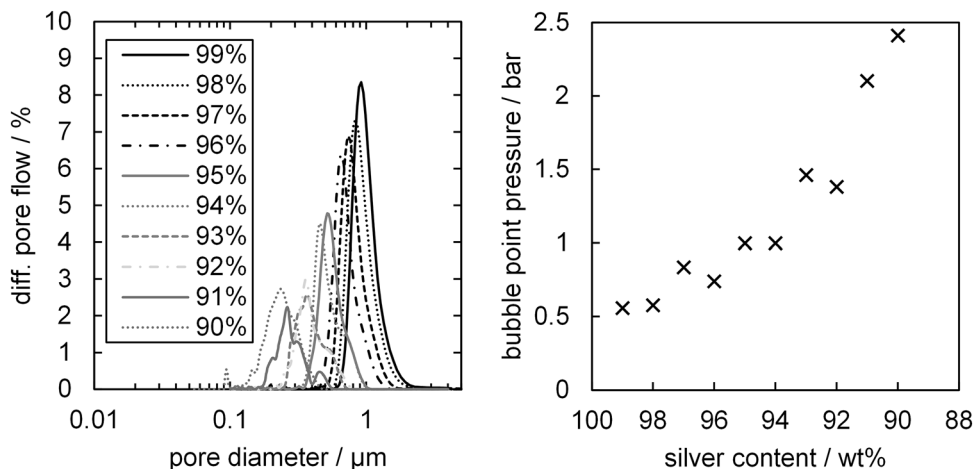
The FIB/SEM images (Fig. 3) of the electrodes provide a look inside the electrodes, revealing details of the pore system. While the bright parts are silver, the darker shapes represent PTFE. The high contrast between these two phases allows for a clear differentiation. It can be seen that the electrode with 99 wt% silver has almost no PTFE inside the pores. With rising PTFE content of the electrode, the silver surface becomes increasingly covered with PTFE. The investigated pores of the electrode with 91 wt% silver appear to be almost completely filled with the PTFE. Interestingly, the shape of the silver structure remains constant and is apparently not influenced by the amount of PTFE. Hence, the PTFE only fills up part of the free space inside the silver skeleton. According to the image analysis, all electrodes consist of silver with approx. 60% volume fraction, while 40% are shared by open pore space and PTFE. However, it has to be kept in mind that the images show only a small area of the whole electrode. The results of the capillary flow porometry reveal that open pathways must exist even for electrodes with high amounts of PTFE. On the other hand, PTFE apparently blocks part of the open silver surface and the electrochemical activity of these electrodes is expected to drop significantly.

In Fig. 4, true and expected electrode densities as well as the BET surface areas are shown. While the expected density, which is calculated based on the true material densities and the weight data, slightly decreases with rising PTFE content, a much stronger decline is observed for the true density determined by pycnometry. This result is an indicator for closed pores within the electrode which cannot be intruded by the helium during pycnometry. The total volume of the closed pores becomes larger with a decreasing amount of silver reaching approximately 20% of the whole electrode volume at 90 wt% silver. As these closed pores should not take part in the electrochemical reaction, the silver catalyst utilization is expected to decrease with rising PTFE content.

The right-hand diagram of Fig. 4 shows that the PTFE content of the electrode does only have minor effects on the BET surface area which is in the range of $0.1 \ m^2 \ g^{-1}$. Only for low silver contents of 92 wt% and less, the surface area slightly increases, however, at rising measuring errors. According to the manufacturer's specifications, the BET surface area of the pristine silver particles is between 0.7 and $1.2 \ m^2 \ g^{-1}$, while the surface area of the PTFE particles corresponds to approx. $13 \ m^2 \ g^{-1}$ derived from the given diameter of the particles. Obviously, the surface area
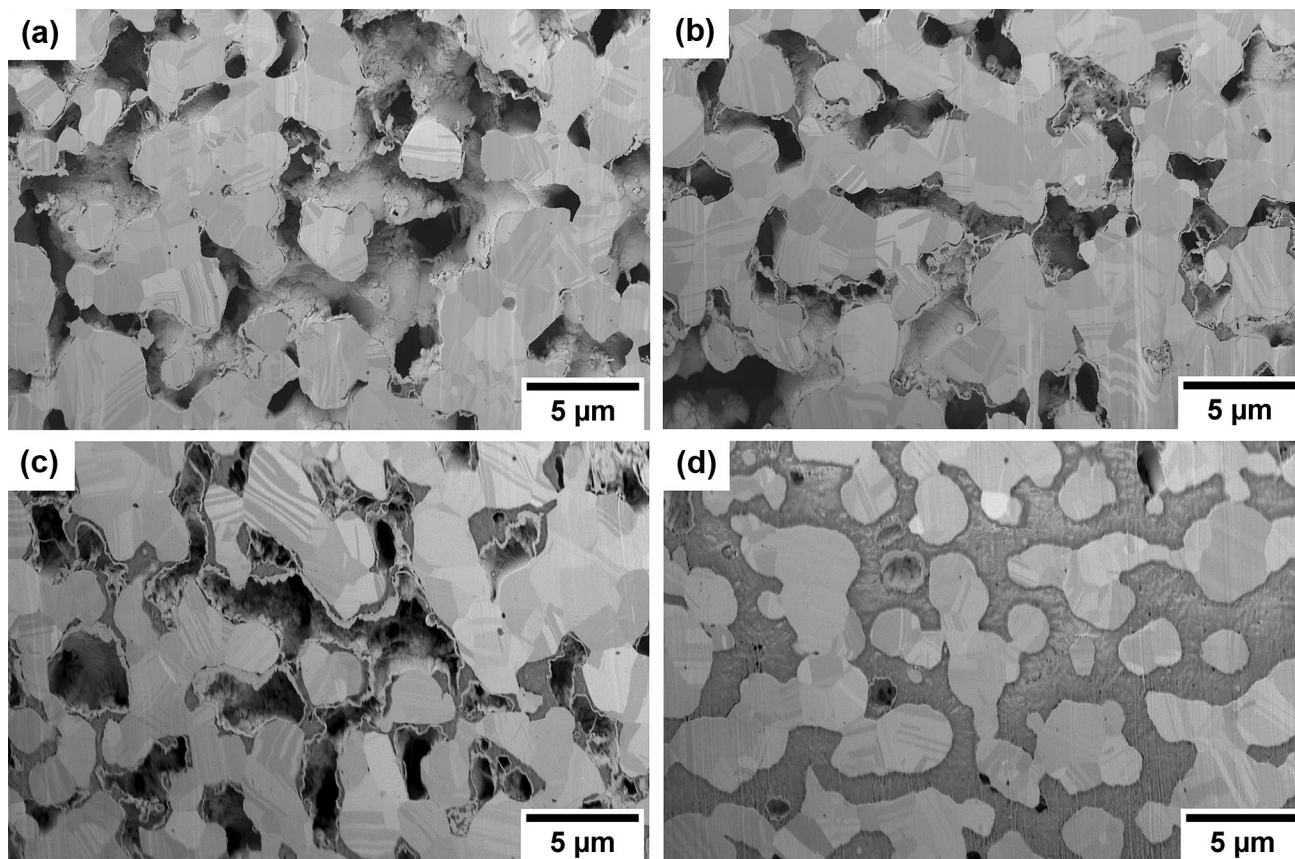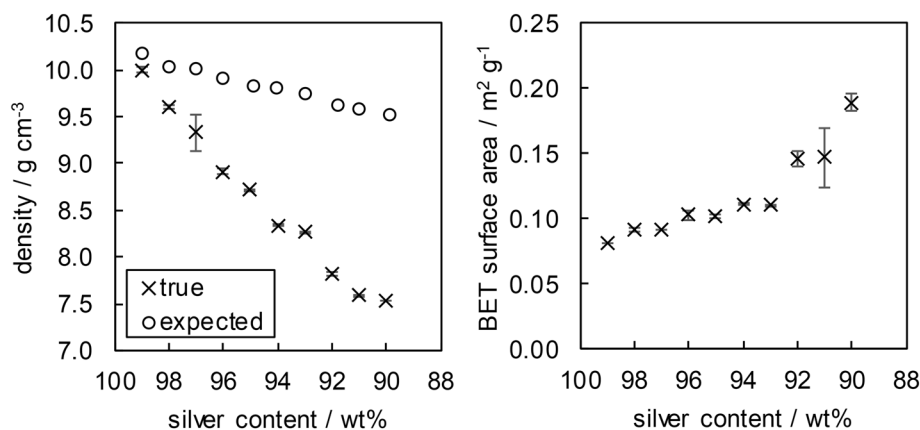

Fig. 3 FIB/SEM images of four electrodes with 99 wt% (**a**), 98 wt% (**b**), 96 wt% (**c**), and 91 wt% (**d**) silver

Fig. 4 Densities and BET surface area as a function of silver content

of the starting materials decreases quite strongly during the fabrication process for which pore filling and sintering might be responsible.

3.2 Influence of PTFE content on ORR activity

The cell resistance for each electrode was determined using electrochemical impedance spectroscopy. The obtained values were in the range between 70 and 200 mOhm without any correlation to the silver content. It is therefore assumed that the conductivities of all electrodes are sufficient for a technical application. The iR compensated polarization curves of the electrodes with different compositions are shown in Fig. 5 revealing a clear trend of the electrochemical performance in dependence of the silver content. While all electrodes exhibit nearly the same overpotential for low current densities, the differences are getting more and more pronounced for current densities above 1 kA m^{-2}. The electrodes with the smallest silver content of 90 wt%, 91 wt%, and 92 wt% reach their limiting current density at 2 kA m^{-2}, 4 kA m^{-2}, and 7 kA m^{-2}, respectively. On the other hand, the 99 wt% electrode does show transport limitations, too, but the effect is less significant. While the lower performance of the electrodes with high PTFE content might be explained by pore blocking and the resulting low filling degree with electrolyte, the high overpotentials for the 99 wt% electrode are most likely the result of a too low PTFE content which allows flooding with electrolyte. The lowest overpotentials are reached with a silver content of 98 wt%, which slightly differs from the optimum of 97 wt% found by Moussallem et al. [5]. Even for the highest applied current density of 8 kA m^{-2}, this electrode does not show any sign of transport limitations. The electrodes with silver contents between 97 and 93 wt% do neither reach a limiting current density, but their overpotentials become slightly larger with decreasing silver content.

The logarithmic diagram in Fig. 5 reveals that the polarization curves can be divided into two regions with different Tafel slopes. The resulting values for the Tafel
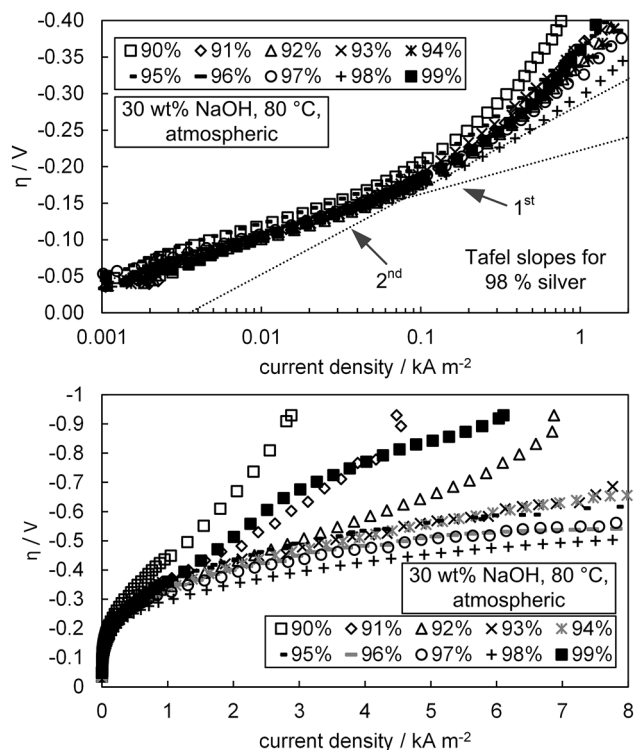

Fig. 5 Overview of polarization curves for electrodes with different silver contents in logarithmic (top) and linear (bottom) representation

slopes are depicted in the left-hand diagram of Fig. 6. It can be seen that the Tafel slopes for the 1st range are not dependent on the silver content and have a constant value of −60 mV dec^{-1}. In the 2nd range, the slopes change as a function of the silver content in the electrode. The best electrode with 98 wt% silver shows a slope of −120 mV dec^{-1}, which slightly decreases for rising PTFE contents with a minimum of −140 mV dec^{-1} at a silver content of 94 wt%.

This observed doubling of the Tafel slope is typical for ORR kinetics in alkaline electrolyte and has been reported by other researchers, too. Sepa et al. observed Tafel slopes

Fig. 6 Tafel slopes (left) and exchange current densities (right) as a function of silver content
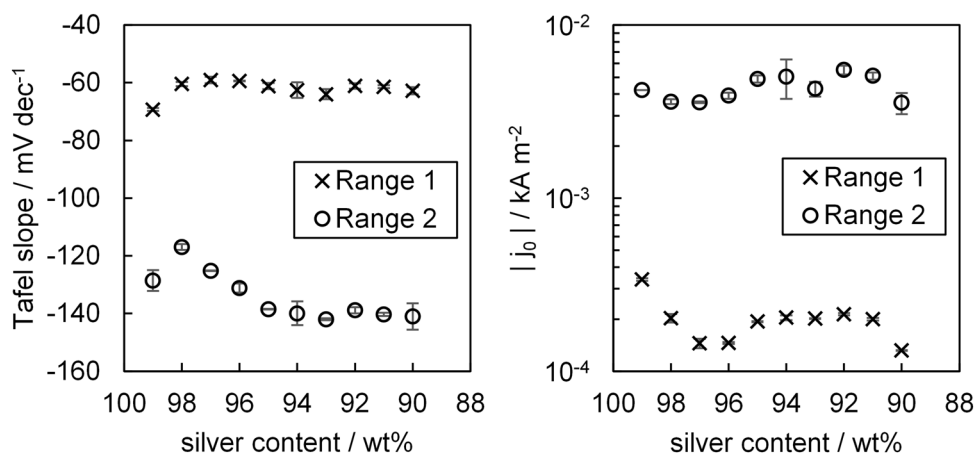
of -60 mV dec^{-1} and -120 mV dec^{-1} for the ORR in aqueous LiOH solution in a temperature range of 5–45 °C [21]. Similar values where observed for different systems using rotating disc electrodes (RDE) [23–25]. At conditions similar to those employed in this study, Blizanac et al. observed slopes of approx. -70 mV dec^{-1} and -130 mV dec^{-1} (0.1 M KOH, 60 °C) on single-crystal surfaces, which were found to be independent of the crystal structure [26]. Pinnow et al. observed values of -80 mV dec^{-1} and -200 mV dec^{-1} with silver/PTFE GDE [6]. In addition to these experimental findings, Shinagawa et al. showed that the two Tafel slopes can also be derived from the microkinetics of the ORR [27].

For the 98% electrode, Tafel slopes close to the true kinetics were determined and almost no influence of transport phenomena can be seen. For decreasing silver content, an increasingly larger transport effect is overlapping resulting in decreasing Tafel slopes. Additionally, the corresponding exchange current densities in both ranges are depicted in the right-hand diagram of Fig. 6 showing only little variation for all tested electrodes. These results indicate that the electrocatalytic activity of the silver particles in the different electrodes is very similar and independent of the particular GDE composition. On the other hand, this means that the overall electrode performance is due to the extent of the three-phase boundary between gaseous oxygen, liquid electrolyte, and solid catalyst, which is determined by the filling degree and the individual liquid pathways in the complex three-dimensional pore system. For the given electrolyte distribution, not only the transport of oxygen but also the local ion activity distribution are of decisive importance as recently shown by Botz et al. [28] through scanning electrochemical microscopy (SECM) measurements.

3.3 Influence of electrolyte pressure on overpotentials during ORR

All experiments discussed so far were obtained at atmospheric pressure (approx. 950 mbar at Clausthal-Zellerfeld)
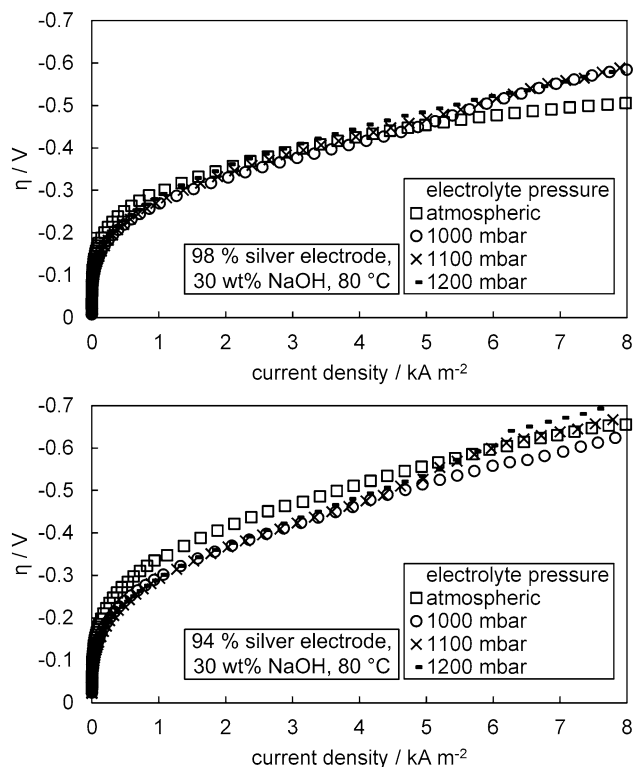

Fig. 7 Polarization curves for two selected electrodes at different electrolyte pressures

with the Gaskatel half-cell. Selected electrodes with silver contents of 98 wt% and 94 wt% were additionally tested under various electrolyte pressure conditions in the specially designed half-cell. The results of these measurements are shown in Fig. 7. It can be seen that for the best performing electrode with a silver content of 98 wt%, an increased electrolyte pressure has a positive effect on the overpotentials for current densities below 3 kA m^{-2}. However, for a current density above approx. 5.5 kA m^{-2} the overpotential increases for higher electrolyte pressures. This result might

be due to an increased filling level of the electrode pores with electrolyte resulting in deteriorated oxygen supply. This interpretation is supported by the fact that for the highest applied electrolyte pressure of 1200 mbar a larger amount of liquid passing from the electrolyte to the gas chamber was observed. For the 94 wt% electrode, a moderately increased electrolyte pressure of 1000 mbar has a clear positive effect on the electrochemical performance in the whole range of current densities. However, at even higher pressures a significant increase of the overvoltage at current densities above 5 kA m^{-2} becomes visible. At the highest pressure of 1200 mbar, this effect becomes so strong that the electrode performance becomes worse than in the cell operated at atmospheric pressure. The increased pressure might lead to a deeper penetration of the electrolyte into the pore system and thus to a better performance. However, at too high pressures parts of the electrode are flooded and larger transport resistances in the electrolyte occur.

During technical application of the GDE in a chlor-alkali electrolysis cell, the electrode should be capable of withstanding a certain pressure difference between gas and electrolyte chamber without loss of performance. A stable electrolysis process is only guaranteed if the electrode is prevented from electrolyte breakthrough. Considering this, an electrode containing 97 wt% silver is still the best compromise between electrochemical performance and practical applicability [5].

4 Conclusion

In the present contribution, a systematic variation of the PTFE content in the production of silver-based GDE and a thorough physical and electrochemical characterization during oxygen reduction was carried out. Based on capillary flow porometry and FIB tomography, it can be concluded that a silver skeleton is build up, while the PTFE is embedded into the free pore space and fills increasingly larger parts of the pore system. In addition, a rising fraction of completely inaccessible parts in the pore system is also formed at too high PTFE contents. Based on LSV measurements, a clear relationship between the formed pore system and the electrochemical performance was identified. On the one hand, all examined electrodes showed very similar electrocatalytic properties in the kinetic regime which can be described with two Tafel slopes showing the typical doubling characteristic for the ORR in alkaline media. On the other hand, the electrode performance at technically relevant higher current density is mainly determined by transport resistances. The best compromise between too strong filling with electrolyte at very low PTFE contents and too severe hydrophobic behavior at higher PTFE fractions offers an electrode

containing 98 wt% silver. For this electrode, no signs of any transport limitation occur even at the highest applied current density of 10 kA m^{-2} under atmospheric electrolyte pressure. However, during application of an increased electrolyte pressure, signs of transport limitations at higher current densities emerged. Overall, the findings revealed that the electrolyte distribution inside the electrode is the key element for understanding the electrochemical performance. Therefore, in situ measurements of a working silver-based GDE should be carried out revealing the electrolyte distribution, as it has been already done for carbon-based GDE used in fuel cells [29]. These measurements are presently carried out in our research groups and will be reported in a forthcoming paper.

Compliance with ethical standards

References

1. Kintrup J, Millaruelo M, Trieu V, Bulan A, Mojica ES (2017) Gas diffusion electrodes for efficient manufacturing of chlorine and other chemicals. Electrochem Soc Interface 26(2):73–76. https://doi.org/10.1149/2.f07172if
2. Jörissen J, Turek T, Weber R (2011) Chlorherstellung mit Sauerstoffverzehrkathoden. Energieeinsparung bei der Elektrolyse. Chem unserer Zeit 45(3):172–183. https://doi.org/10.1002/ciuz.201100545
3. Moussallem I, Jörissen J, Kunz U, Pinnow S, Turek T (2008) Chlor-alkali electrolysis with oxygen depolarized cathodes: history, present status and future prospects. J Appl Electrochem 38(9):1177–1194. https://doi.org/10.1007/s10800-008-9556-9
4. Furuya N, Aikawa H (2000) Comparative study of oxygen cathodes loaded with Ag and Pt catalysts in chlor-alkali membrane cells. Electrochim Acta 45(25–26):4251–4256. https://doi.org/10.1016/s0013-4686(00)00557-0
5. Moussallem I, Pinnow S, Wagner N, Turek T (2012) Development of high-performance silver-based gas-diffusion electrodes for chlor-alkali electrolysis with oxygen depolarized cathodes. Chem Eng Process: Process Intensif 52:125–131. https://doi.org/10.1016/j.cep.2011.11.003
6. Pinnow S, Chavan N, Turek T (2011) Thin-film flooded agglomerate model for silver-based oxygen depolarized cathodes. J Appl

Electrochem 41(9):1053–1064. https://doi.org/10.1007/s10800-011-0311-2

7. Chavan N, Pinnow S, Polcyn GD, Turek T (2015) Non-isothermal model for an industrial chlor-alkali cell with oxygen-depolarized cathode. J Appl Electrochem 45(8):899–912. https://doi.org/10.1007/s10800-015-0831-2

8. Frania P (2016) Herstellung, Analyse und Optimierung von Sauerstoffverzehrkathoden mit elektrochemisch abgeschiedenem Silberkatalysator zum Einsatz in der Chlor-Alkali-Elektrolyse. Dissertation, 1. Auflage. Technische Universität Dortmund; Verlag Dr. Hut

9. Zils S, Timpel M, Arlt T, Wolz A, Manke I, Roth C (2010) 3D visualisation of PEMFC electrode structures using FIB nanotomography. Fuel Cells 10(6):966–972. https://doi.org/10.1002/fuce.201000133

10. Danner T, Eswara S, Schulz VP, Latz A (2016) Characterization of gas diffusion electrodes for metal-air batteries. J Power Sources 324:646–656. https://doi.org/10.1016/j.jpowsour.2016.05.108

11. Neumann M, Osenberg M, Hilger A, Franzen D, Turek T, Manke I, Schmidt V (2019) On a pluri-Gaussian model for three-phase microstructures, with applications to 3D image data of gas-diffusion electrodes. Comput Mater Sci 156:325–331. https://doi.org/10.1016/j.commatsci.2018.09.033

12. Arvay A, Yli-Rantala E, Liu C-H, Peng X-H, Koski P, Cindrella L, Kauranen P, Wilde PM, Kannan AM (2012) Characterization techniques for gas diffusion layers for proton exchange membrane fuel cells—a review. J Power Sources 213:317–337. https://doi.org/10.1016/j.jpowsour.2012.04.026

13. Salzer M, Spettl A, Stenzel O, Smått J-H, Lindén M, Manke I, Schmidt V (2012) A two-stage approach to the segmentation of FIB-SEM images of highly porous materials. Mater Charact 69:115–126. https://doi.org/10.1016/j.matchar.2012.04.003

14. Moussallem I (2011) Development of Gas Diffusion Electrodes for a New Energy Saving Chlor-Alkali Electrolysis Process. Dissertation, Institute of Chemical Process Engineering, TU Clausthal

15. Turek TMoussallem I, Bulan A et al. (2010) Oxygen-consuming electrode and method for its production (EP20110169579 20110610)

16. Schindelin J, Arganda-Carreras I, Frise E, Kaynig V, Longair M, Pietzsch T, Preibisch S, Rueden C, Saalfeld S, Schmid B, Tinevez J-Y, White DJ, Hartenstein V, Eliceiri K, Tomancak P, Cardona A (2012) Fiji: an open-source platform for biological-image analysis. Nat Methods 9:676. https://doi.org/10.1038/nmeth.2019

17. Bratsch SG (1989) Standard electrode potentials and temperature coefficients in water at 298.15 K. J Phys Chem Ref Data 18(1):1–21. https://doi.org/10.1063/1.555839

18. Balej J (1985) Water vapour partial pressures and water activities in potassium and sodium hydroxide solutions over wide concentration and temperature ranges. Int J Hydrog Energy 10(4):233–243. https://doi.org/10.1016/0360-3199(85)90093-x

19. Balej J (1996) Activity coefficients of aqueous solutions of NaOH and KOH in wide concentration and temperature ranges. Collect Czech Chem Commun 61(11):1549–1562. https://doi.org/10.1135/cccc19961549

20. Tromans D (2000) Modeling oxygen solubility in water and electrolyte solutions. Ind Eng Chem Res 39(3):805–812. https://doi.org/10.1021/ie990577t

21. Sepa DB, Vojnovic MV, Vracar LM, Damjanovic A (1986) Apparent enthalpies of activation of electrodic oxygen reduction at platinum in different current density regions—II. Alkaline solution. Electrochim Acta 31(1):97–101. https://doi.org/10.1016/0013-4686(86)80068-8

22. Mugele FBaret J-C (2005) Electrowetting: from basics to applications. J Phys: Condens Matter 17(28):R705–R774. https://doi.org/10.1088/0953-8984/17/28/r01

23. Blizanac BB, Ross PN, Markovic NM (2007) Oxygen electroreduction on Ag(111): the pH effect. Electrochim Acta 52(6):2264–2271. https://doi.org/10.1016/j.electacta.2006.06.047

24. Obradović MD, Grgur BN, Gojković SL, Vračar LM (2006) Enhancement of the electrochemical reduction of oxygen at platinum by nickel underpotential deposition. J Solid State Electrochem 11(1):77–83. https://doi.org/10.1007/s10008-005-0072-0

25. Chatenet M, Genies-Bultel L, Aurousseau M, Durand R, Andolfatto F (2002) Oxygen reduction on silver catalysts in solutions containing various concentrations of sodium hydroxide—comparison with platinum. J Appl Electrochem 32(10):1131–1140. https://doi.org/10.1023/a:1021231503922

26. Blizanac BB, Ross PN, Marković NM (2006) Oxygen reduction on silver low-index single-crystal surfaces in alkaline solution: rotating ring disk(Ag(hkl)) studies. J Phys Chem B 110(10):4735–4741. https://doi.org/10.1021/jp056050d

27. Shinagawa T, Garcia-Esparza AT, Takanabe K (2015) Insight on Tafel slopes from a microkinetic analysis of aqueous electrocatalysis for energy conversion. Sci Rep 5:13801. https://doi.org/10.1038/srep13801

28. Botz A, Clausmeyer J, Öhl D, Tarnev T, Franzen D, Turek T, Schuhmann W (2018) Local activities of hydroxide and water determine the operation of silver-based oxygen depolarized cathodes. Angew Chem Int Ed 57(38):12285–12289. https://doi.org/10.1002/anie.201807798

29. Muirhead D, Banerjee R, George MG, Ge N, Shrestha P, Liu H, Lee J, Bazylak A (2018) Liquid water saturation and oxygen transport resistance in polymer electrolyte membrane fuel cell gas diffusion layers. Electrochim Acta 274:250–265. https://doi.org/10.1016/j.electacta.2018.04.050

Affiliations

David Franzen[1] · **Barbara Ellendorff[1]** · **Melanie C. Paulisch[2]** · **André Hilger[2]** · **Markus Osenberg[2]** · **Ingo Manke[2]** · **Thomas Turek[1]**

[1] Institute of Chemical and Electrochemical Process Engineering, Clausthal University of Technology, Clausthal-Zellerfeld, Germany

[2] Institute of Applied Materials, Helmholtz-Zentrum Berlin for Materials and Energy, Berlin, Germany